Flow Properties of Suspensions with High Solids Concentration

E. C. GAY and P. A. NELSON

Argonne National Laboratory, Argonne, Illinois

and W. P. ARMSTRONG

Washington University, St. Louis, Missouri

Equations were developed for evaluating the laminar flow behavior of high-solids suspensions from the physical properties of the liquid and solid components. A technique was developed for calculating suspension flow rates as a function of pressure drop. The technique is applicable to the design of pipe lines. Flow measurements were made in pipe-line viscometers of a unique design that minimized entrance and exit effects. Experimental flow data were obtained for suspensions consisting of nickel, alumina, copper, or glass solids in sodium, xylene, or glycerine vehicles with solids concentrations of 28 to 55 vol. %. The basis for the correlation of the data was an analytical investigation of the flow behavior that considered the particle-particle interaction that takes place in a settled suspension. The correlation equations fit all systems investigated. They take into account the effects of liquid viscosity, liquid and solid densities, particle size, size distribution, particle surface area, volume fraction of solids in the suspension, and volume fraction of solids at maximum settled conditions.

The design of pipe flow systems for suspensions of high-solids content requires a detailed knowledge of the non-Newtonian laminar flow properties (*1* to *3*) of the suspension. Normally, the flow properties of suspensions of interest have to be determined experimentally over a wide range of flow rates. Mathematical models, such as the well-known Bingham plastic model, that relate shear stress to shear rate are helpful in describing the flow properties of non-Newtonian fluids. However, for most suspensions (particularly where particle size, shape, and degree of dispersion differ) the parameters in the mathematical models have to be measured for each suspension.

The objective of the present investigation was to provide a means of predicting flow behavior by making a general rheological study of solid-liquid suspensions and relating suspension viscosity to physical properties of the solids and liquids. Suspensions of high-solids content were of particular interest in this study, since little work has been done on such systems.

Other investigators have proposed equations for relating suspension viscosity to properties of the constituents, but none of the investigations have been concerned simultaneously with the non-Newtonian flow region and suspensions of high-solids content.

Robinson (*4*) extended the Einstein equation to higher concentrations by introducing the concept that the specific viscosity ($\eta_r - 1/\eta_r$) is inversely proportional to the volume of free liquid in the suspension. This volume of free liquid may be defined as the difference between the total volume of the suspension and an effective volume of solids.

Vand (*5*) derived the theoretical relationship

$$\ln \eta_r = \frac{a \phi}{1 - k\phi}$$

where $k = 0.60937$. The parameter a is a shape factor, and must be 2.5 for spheres. Vand derived this equation by taking into account the interaction of the solid particles and applying the Arrhenius formula. Mooney (*6*) described the interaction between particles at higher concentration as essentially a crowding effect. Mooney suggests $a = 2.5$, and $1.35 < k < 1.91$.

Landel (*7*) proposed an equation for suspension viscosity that is applicable to very high solids concentrations, but the equation was limited to the flow region of constant viscosity observed at low shear rates. Non-Newtonian flow was observed by Landel, but no attempt was made to calculate the non-Newtonian viscosity.

Williams (*8*) noted that suspensions with particles less than 1μ in size exhibit non-Newtonian behavior. This non-

Newtonian behavior is caused by a flocculated structure of the dispersed particles in the suspending medium. Thomas (*9, 10*) has correlated viscosity measurements of flocculated suspensions with the Bingham plastic model, but the highest solids concentration used in that investigation was 0.23 volume fraction solids. For these suspensions, Thomas was able to calculate the yield stress and coefficient of rigidity from physical properties of the constituents for a wide range of materials.

In this investigation, a doctoral research project, a survey of the application of suspensions as fluid fuels for nuclear reactors was carried out. This survey and other references on suspension flow research are given elsewhere (*11*).

DEVELOPMENT OF MATHEMATICAL MODEL

A mathematical model for the shear stress-shear rate relationship was developed for high-solids suspensions in pipe flow. The particles of such suspensions become interlocked in the absence of flow. Also, yield stress was observed for all suspensions in the present investigation, and has been reported by numerous other investigators for concentrated suspensions (*3, 9, 10, 12* to *14*). Therefore, it was recognized that the shear stress-shear rate expression must involve a term for yield stress.

For flow to begin in any local region, the particles must first be moved apart in the direction normal to the plane of flow to allow slippage between the planes. The required volume displacement per unit area in the plane of flow is directly proportional to the particle diameter. The space available for particle movement per unit volume of space is the difference between the maximum obtainable solids volume fraction for the system, ϕ_m, and the actual solids volume fraction, ϕ. The yield stress, τ_y, required to initiate flow is directly proportional to the normal force per unit area required to separate two adjacent planes of particles sufficiently to allow flow. This normal force was assumed to be proportional to the displacement required for flow (that is proportional to the particle diameter, D_p), and inversely proportional to the space available to accommodate the displacement (that is inversely proportional to $\phi_m - \phi$). Therefore, the yield stress is expressed by the relationship:

$$\tau_y = A\left(\frac{D_p}{\phi_m - \phi}\right) \tag{1}$$

The constant A is dimensional, and must take into account other factors that affect the yield stress such as the volume fraction of solids, the sphericity of the particles, and the particle size distribution. Therefore, A was determined in this investigation from an empirical correlation of these factors.

To obtain the shear stress-shear rate relationship for pipe flow of high-solids suspensions, it was assumed that the equation

$$\tau_{rz} - \tau_y = \frac{\eta_\infty}{g_c} G + \theta \tag{2}$$

was applicable for laminar flow and for a suspension having a yield stress, where τ_{rz} is the shear stress in the axial direction, z, of the test pipe and at a distance, r, from the axis; η_∞ is the viscosity coefficient; G is the shear rate; and θ is the shear stress needed to overcome particle-particle interactions due to suspension flow. A similar expression was first used by Goodeve (*15*) for flocculated suspensions.

It is desirable to relate θ to physical properties of the solids. Considering spherical particles of diameter D_p, the number of particle-particle contacts per unit area in a layer one particle thick is $D_p n_c$, where n_c is the number of particle-particle contacts per unit volume. The transfer of momentum from one layer to another per unit surface area and time is

$$\theta = F_s D_p n_c \tag{3}$$

where F_s is the force necessary to overcome interparticle contact.

The rate of formation of contacts is a second-order process, since two particles are necessarily involved. However, the rate of destruction of contacts is simply proportional to the number of contacts. Thus,

$$\frac{dn_c}{dt} = KN^2 - \beta n_c \tag{4}$$

where N is the number of particles per unit volume. At steady state, the rates of formation and breaking of contacts is equal. Hence,

$$n_c = \frac{KN^2}{\beta} \tag{5}$$

Since the particles are brought into contact by their relative motion due to shear, K is proportional to the shear rate, G. Manley and Mason (*16*) have shown that the two-body collision frequency per unit volume, f, is

$$f = \frac{2}{3} D_p^3 N^2 G \tag{6}$$

Therefore,

$$K = \frac{2}{3} D_p^3 G \tag{7}$$

Particle-particle contact is destroyed by relative motion due to shear, which suggests a direct proportionality between β and G. However, in order to obtain a viscosity equation that will express the pseudoplastic behavior that has been observed at low shear rates for high-solids suspensions, the rate constant, β, for the breaking of contacts is expressed as a linear function of G rather than as a direct proportion. Thus,

$$\beta = \beta_0 + \beta_1 G \tag{8}$$

It should be noted that β_0 has a negligible effect except at low values of G, or at high solids concentrations. The constant β_1 can be evaluated from the work of Manley and Mason (*16*) for conditions such that β_0 can be ignored. From the expression presented (*16*) for the time, t_c, spent by one sphere in collision with other spheres, $t_c = 4\phi/G$. Also, noting that by definition $t_c = 1/\beta$,

$$\beta_1 = \frac{1}{4\phi} \tag{9}$$

From the above transformations, and noting that $N = 6\phi/\pi D_p^3$, the following relation is obtained:

$$\tau_{rz} - \tau_y = \frac{\eta_\infty G}{g_c} + \frac{96\,\phi^3 F_s G}{\pi^2 D_p^2 (4\beta_0\phi + G)} \tag{10}$$

From this relation, the suspension viscosity coefficient, $(\tau_{rz} - \tau_y) g_c/G$, may be expressed by

$$\eta = \eta_\infty + \frac{g_c B}{4\beta_0\phi + G} \tag{11}$$

where

$$B = 96\,\phi^3 F_s/\pi^2 D_p^2 \tag{12}$$

At very low shear rates, $G << 4\beta_0\phi$, and Equation (11) reduces to

$$\beta_0 = \frac{1}{4\phi}\left(\frac{g_c B}{\eta_0 - \eta_\infty}\right) \tag{13}$$

where η_0 = the viscosity parameter at the initiation of

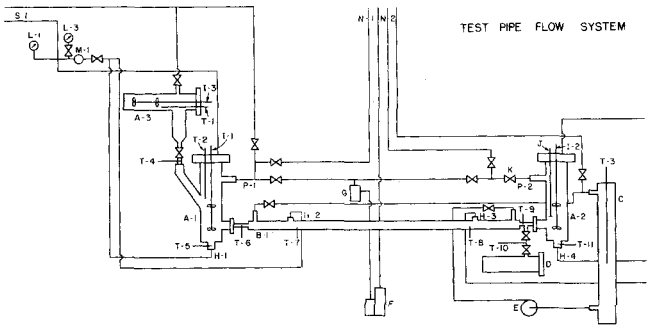

Fig. 1. Test pipe flow system in configuration used for sodium suspensions. A-1. supply reservoir, A-2. receiving vessel, A-3. mixing vessel, B-1. test pipe, C. heating oil reservoir, D. unloading vessel, E. centrifugal pump, F. vacuum pump, C. cold trap, H1-H4. pressure transducers, I1-I2. mixing shafts, J. electrical probe, K. back pressure regulating valve, L1-L4, Bourden tube pressure gauges, M1-M2. pressure relief disks, N1-N2. hydrogen venting lines, P1-P2. vacuum lines, S1-S2. Argon pressure lines, T1-T11. Thermocouples, V. stainless steel valves.

flow. Substituting Equation (13) into Equation (11),

$$\eta = \eta_\infty + \frac{\eta_0 - \eta_\infty}{1 + \left(\frac{\eta_0 - \eta_\infty}{g_c B}\right) G} \qquad (14)$$

This is the desired relationship between the suspension viscosity and the shear rate. It is necessary, however, to express the parameters, B, η_0, and η_∞ in terms of the physical properties of the particles and the liquid vehicle.

Because of the difficulty of defining F_s in Equation (12) in terms that are easily measurable, an expression for B was found by dimensional analysis. The parameters B and τ_y are related in that they have the same dimensions and are both dependent on interparticle forces. Therefore, τ_y should be an important factor in an empirical expression for B. In addition, B is a shear stress factor for particles in motion and must, therefore, take into account viscous and momentum forces. The maximum obtainable solids fraction, ϕ_m, and the volume fraction available for particle movement, $\phi_m - \phi$, were also considered to be important. By dimensional analysis,

$$B = f[\phi_m,\ \phi_m - \phi, \tau_y, \mu, \rho_p,\ D_p] \qquad (15)$$

and

$$\frac{B}{\tau_y} = C\ \phi_m{}^k\ (\phi_m - \phi)^l \left(\frac{\mu^2}{D_p{}^2\ \rho_p\ \tau_y}\right)^m \qquad (16)$$

where ρ_p is the density of the suspension or paste.

An expression for η_0 was taken from the work of Landel (7), who found that the suspension viscosity at low shear rates may be expressed by

$$\eta_0 = \mu \left(\frac{\phi_m}{\phi_m - \phi}\right)^{2.5} \qquad (17)$$

for a number of suspensions at high-solids content over a wide range of physical properties. Equation (17) reduces to

$$\eta_0 = \mu\ (1 + 2.5\phi/\phi_m) \qquad (18)$$

for very dilute suspensions. This is the Einstein equation, except that ϕ/ϕ_m is substituted for ϕ.

A relationship was sought for η_∞ that would also reduce to Equation (18) for dilute solutions, in order that the correlation results might have significance beyond the range of variables studied in this investigation. The following expression fulfills this requirement, and agrees well with the experimental data:

$$\eta_\infty = \mu\ \exp\left\{\left[2.5 + \left(\frac{\phi}{\phi_m - \phi}\right)^n\right]\frac{\phi}{\phi_m}\right\} \qquad (19)$$

where $n = 0.48$ was determined from a least-squares analysis of the data as discussed below.

In Equation (19), the expression, $\phi/(\phi_m - \phi)$, is equal to $(\phi/\phi_m)/(1 - \phi/\phi_m)$. Thus, η_∞/μ, in Equation (19), is a function of ϕ/ϕ_m alone.

The expressions for τ_y and η were derived by consideration of particles of uniform size. However, these expressions were applied to suspensions containing particles of nonuniform size by accounting for the particle size distribution in terms A and B, which are related to particle interaction.

To evaluate τ_y and η, and thus obtain the desired relationship for expressing the flow behavior of suspensions, it is necessary to evaluate the constants A, C, k, l, m, and n in Equations (1), (16), and (19). This was done in this investigation by correlation of viscosity measurements for well defined suspensions.

EXPERIMENTAL PROCEDURE

Viscosity Measurements

A pipe flow system was designed and constructed to obtain experimental viscosity data for suspensions of high solids content. The findings of other investigators for flow through horizontal conduits were considered in the design. The system was capable of handling liquid sodium suspensions at high temperature, as well as suspensions containing high-viscosity organic vehicles.

A major factor in measuring low rates of concentrated suspensions is the influence of entrance, exit, and wall effects on the pressure gradient in the test pipes (17 to 22). Particular attention was given to the design of the test pipes in order to minimize these effects. It has been shown (22) that laminar wall effects are negligible for flocculated suspensions of particles in the micron size range flowing through tubes from ⅛ to 1 in. in diameter. It has also been shown that the laminar flow entrance effect for pseudo-plastic non-Newtonian fluids decreases from that found for Newtonian fluids as the non-Newtonian character is increased (23). The maximum entrance correction for Newtonian fluids at the transition Reynold's number of 2,100 is about 5% for tubes with a length-to-diameter ratio of 1,000. The entrance correction is always smaller than 5% for lower flow rates, and for non-Newtonian behavior.

Laminar flow rheological properties were determined in this study from pressure drop-flow rate measurements using jacketed, horizontal pipe viscometers constructed of stainless steel tubing. The pipe flow system included a means of loading the suspension into a supply reservoir under an inert atmosphere, an oil recirculating system for maintaining a constant temperature in the jacketed pipe viscometer section, an electric probe to determine sodium suspension height in a receiving reservoir, differential pressure transducers to determine suspension flow rates and test-pipe pressure differentials, argon pressure sources to force the suspension through the system, and a means of mixing the suspension in the reservoirs. A schematic diagram of the pipe flow system is shown in Figure 1. The viscometers were fitted with pressure taps of unique design

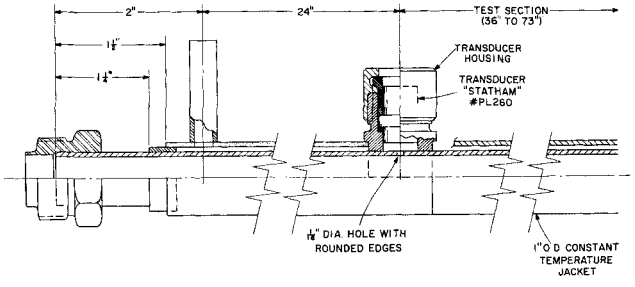

Fig. 2. Test pipe section showing pressure tap and constant temperature jacket.

(Figure 2) that could measure pressure gradients without disturbing the flow. These pressure taps were located 26 in. from the ends of the viscometers to eliminate end effects. Three different viscometers of this design were used, having distances between the pressure taps of 36, 72, and 73 in., and inside diameters of 0.624, 0.269 and 0.627 in., respectively.

During a viscosity measurement, the suspension in the supply reservoir was agitated continuously by two 2½ in. diameter impellers spaced 4½ in. apart on a single shaft. The shaft extended through a stuffing box, and was driven at 300 to 400 rev./min. Suspensions could be mixed in either reservoir and moved by pressure difference in either direction.

Flow rates of the sodium-vehicle suspensions were measured by determining head changes in the sealed reservoirs with electric probe measurements, or by monitoring differences in the pressure recorded by the reservoir pressure transducers. In the case of the organic-vehicle suspensions, protection from air was not required, so only one reservoir was needed. The flow rate of these suspensions was determined from the weight of the suspensions collected at the end of the test pipe during a measured time interval. A sufficient number of pressure drop readings vs. flow rate were obtained to yield a continuous, smooth curve. Occasionally, after a set of data had been plotted, it was necessary to make reruns to check spurious data.

Characterization of Suspensions

Values of the following physical properties were needed to correlate the theoretical viscosity equations with measurements of suspension viscosities: solids density and surface area, volume fraction solids, maximum attainable volume fraction solids, particle diameter, and particle size distribution. Details of the methods used for measuring these values are presented in the doctoral dissertation based on this research (*11*). A brief description of the methods is given below.

Samples of the suspension were obtained directly from the test-pipe section at the end of each run and the solids concentration was determined for each sample. In the case of runs with sodium-vehicle suspensions, it was necessary to unfasten a coupling to obtain a sample. These samples were necessary to insure that the solids concentration during the flow measurements was the same as that calculated from the ingredients in the batch of material. The sodium samples were analyzed by dissolving the material in methyl alcohol, filtering the solids, diluting an aliquot portion with water, and titrating with standard acid. The organic samples were weighed, washed with water or methyl alcohol, filtered, and dried. The solids were weighed and the solid weight fraction determined. In all cases, the solids concentration of the samples was within 1% of that calculated from the ingredients in the batch of material.

The density of the solid particles, which was needed to calculate the solids volume fraction, was measured by xylene displacement in calibrated 250 ml. volumetric flasks, and checked with an air-comparison pycnometer (*24*). Both techniques gave the same values of density within the experimental error.

The maximum volume fraction solids was determined by centrifuging slurries of the various particle systems. This technique has been applied by other investigators (*7*), and has been shown to give good estimates of the maximum solids fraction in a number of vehicles. Care was taken in these measurements to insure reproducibility, since small errors in the measurement of the maximum fraction solids would result in large errors in calculated viscosities for concentrated suspensions. Particle surface areas were determined by measurements of nitrogen gas adsorbed by the solids. A Perkin-Elmer shell model 212 sorptometer was used for these measurements (*25*).

Particle diameters and size distributions were measured with a Coulter counter (*26*). The diameters measured by this instrument were equivalent spherical diameters. The size distributions were closely approximated by the logarithmic normal expression (*27*), and could be characterized by two parameters: the geometric mean diameter, and the logarithmic standard deviation.

EXPERIMENTAL RESULTS

Flow measurements were obtained with suspensions of 28.0 to 55.0 vol. % solids consisting of sodium-nickel, xylene-nickel, xylene-alumina, glycerin-alumina, glycerin-nickel, glycerin-copper, glycerin-no. 660 glass spheres and glycerin-no. 380 glass spheres. A summary of the suspension characteristics is given in Table 1.

A total of 145 viscosity measurements were made on fourteen different suspensions. The pressure drops measured ranged from 0.8 to 33 lb./sq.in. The pressure measuring transducers were carefully calibrated to give an accuracy of about ± 1% in the lower range of pressure drops and considerably greater accuracy in the higher ranges where most of the runs were carried out. However, the flow rates for a given pressure drop in some of the systems were reproducible to no better than ± 10% accuracy. Apparently, this lack of reproducibility was caused by slight variations in solids concentration.

For each measurement of flow and pressure drop, the wall shear stress was calculated from the relationship:

$$\tau_w = \frac{D\Delta P}{4L} \tag{20}$$

Similarly, the shear rates at the wall were calculated from a log-log plot of the function $(32Q/\pi D^3)$ vs. τ_w and the Rabinowitsch equation,

$$G_w = \left(\frac{3+b}{4}\right)\left(\frac{32Q}{\pi D^3}\right) \tag{21}$$

where

$$b = \frac{d \ln\left(\frac{32Q}{\pi D^3}\right)}{d \ln\left(\frac{D\Delta P}{4L}\right)} \tag{22}$$

Table 1. Suspension Characteristics

Vehicle Characteristics			Solids Characteristics					
				Density*	Particle Size†			
Material	Temp., °C.	Visc., cP.	Material	g./cc.	D_p, u	σ_g	ξ	ϕ_m‡
sodium	150	0.54	nickel	7.32	10.5	2.02	0.118	0.317
m-xylene	21	0.61	nickel	7.32	10.5	2.02	0.118	0.374
m-xylene			alumina	3.48	12.0	1.66	0.164	0.468
glycerine	25	954	copper	8.58	26.0	1.53	0.108	0.327
glycerine			nickel	7.32	10.5	2.02	0.118	0.374
glycerine			alumina	3.48	12.0	1.66	0.164	0.550
glycerine			No. 660 glass	2.33	64.0	1.21	1.0	0.713
glycerine			No. 380 glass	2.31	34.5	1.19	1.0	0.670

* Measured by Xylene displacement
† D_p = geometric mean diameter, σ_g = geometric standard deviation, ξ = shape factor
‡ ϕ_m = maximuu volume fraction solids in the vehicle

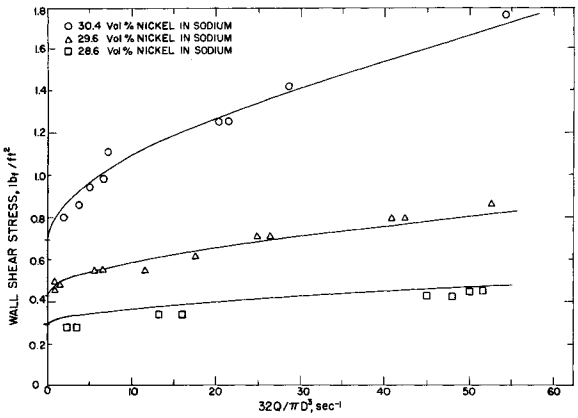

3a

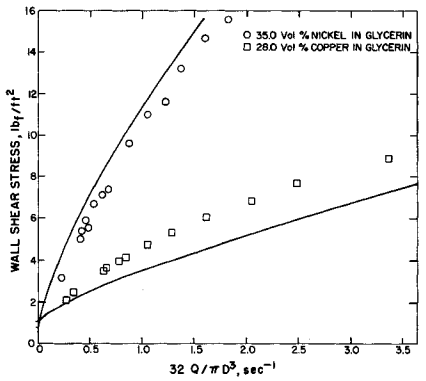

3b

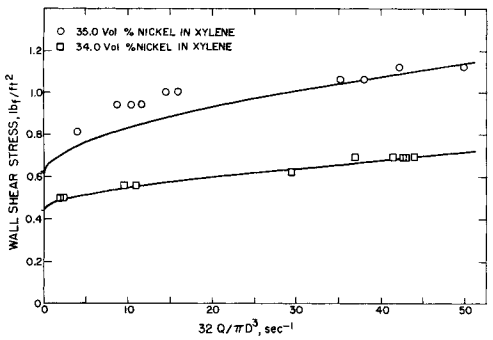

3c

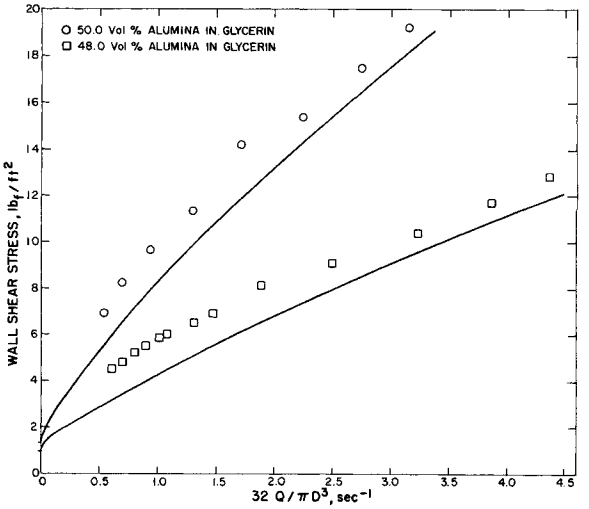

3d

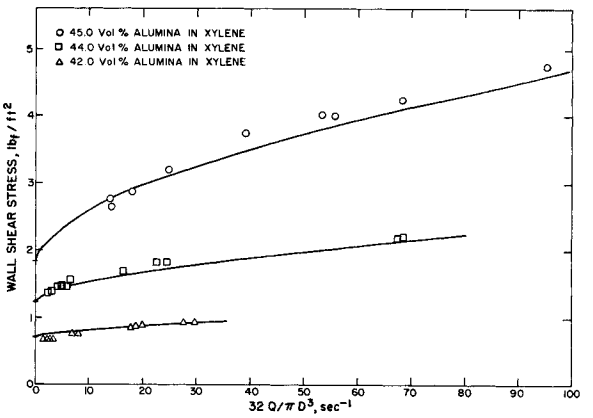

3e

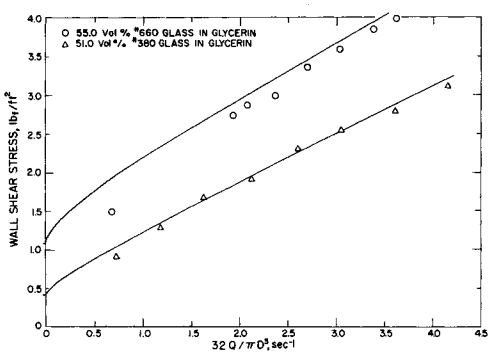

3f

Fig. 3. Wall shear stress vs. flow parameter ($32Q/\pi D^3$, sec.$^{-1}$). The curves were calculated from Equation (32) and physical properties of the solids and vehicles.

The resulting values of G_w and τ_w are tabulated elsewhere (*11*). The shear stress at the wall was plotted vs. $32Q/\pi D^3$ in Figure 3, and vs. the wall shear rate in Figure 4. The lines in these plots were calculated from the correlation equations discussed in the next section. The data in some of these plots are for several pipe sizes and pipe lengths, yet they are evenly distributed about the curve of best fit. This indicates no time effects, no slippage at the pipe wall, and no entrance and exit effects. It was also demonstrated that the data fit the generalized friction factor plot proposed by Metzner (*28*) (see reference *11* for this plot).

The plots of τ_w vs. G_w, for all of the systems, resulted in curves that indicated a yield stress, a pseudoplastic region at low shear rate, and a Bingham plastic region at high shear rate. This is in general agreement with the semitheoretical relation

$$\tau_w - \tau_y = \frac{\eta_\infty}{g_c} G_w + \frac{\left(\frac{\eta_0 - \eta_\infty}{g_c}\right) G_w}{1 + \left(\frac{\eta_0 - \eta_\infty}{g_c B}\right) G_w} \qquad (23)$$

which is derived from Equations (10), (11), and (14).

An attempt was made to determine approximate experimental values of η_0, η_∞, τ_y, and B. Although there was not sufficient data in most of the runs at low shear rates for accurate determination of η_0, the slopes of the curves appeared to be in agreement with Equation (17) for η_0. This agreement aided the graphical determination of an experimental value for τ_y. In theory, experimental values of B and η_∞ can be calculated from the following relationship, that can be derived from Equation (23) for high values

of G_w:

$$\tau_w = \frac{\eta_\infty}{g_c} G_w + \tau_i \tag{24}$$

where

$$\tau_i = \tau_y + B \tag{25}$$

At high wall shear rates, the experimental τ_w vs. G_w data of Figure 4 appear to fit the straight line of Equation (24), and thus permit determination of experimental values of η_∞, τ_i, and B. However, the values so obtained for τ_i and B are considerably different from those calculated from the general correlation discussed in the next section, even for cases where the correlation equation fits the data accurately. Therefore, it was concluded that graphical determinations of τ_i and B are not reliable, and that η_∞ can be determined graphically only for systems where sufficient data are available at very high wall shear rates.

CORRELATION OF DATA

Expressions in terms of easily measured physical properties were sought for τ_y, B, η_0, and η_∞ in the semitheoretical Equation (23). Landel's expression, Equation (17), was accepted for η_0 as discussed above. Expressions for the remaining parameters, τ_y, B, and η_∞, in the form of Equations (1), (16), and (19) respectively, were found by a combination of trial-and-error and least-squares correlation of the experimental data.

To accomplish this correlation, a computer program was devised to find the minimum value for the correlation function ψ:

$$\psi = \sum_{i=1}^{145} \left[\left(\frac{\tau_{wc}}{\tau_{wo}} \right) - 1 \right]^2 \tag{26}$$

where τ_{wc} and τ_{wo} are the calculated value and corresponding observed value, respectively, of the wall shear stress for each of the 145 experimental runs.

It should be noted that this method minimizes the sum of the squares of the percentage difference between the calculated value, τ_{wc}, and the observed value, τ_{wo}, rather than minimizing the sum of the squares of the absolute difference between the values. This method was used because the observed values of τ_w varied by a factor of 70, and were reproducible to within approximately $\pm$ 10% regardless of the absolute value of τ_w. The calculated values of τ_w for substituting in Equation (26) were obtained from Equation (23), with appropriate expressions substituted for τ_y, B, η_0, and η_∞. These expressions contained sixteen parameters, including C, k, l, m, and n of Equations (16) and (19), as well as parameters in various trial expressions for A of Equation (1). Values of G_w used in calculating τ_w from Equation (23) were determined by the graphical technique discussed in the previous section.

The computer program found the optimum value of the parameters for a minimum value of ψ by a method given by Marquardt (29). As many as nine parameters were allowed to vary at once, while the others were fixed. After many trial-and-error attempts, the following equations were found to be the most compatible with the data and the theory:

$$\tau_y = 200 \left(\frac{D_p}{\phi_m - \phi} \right) \left(\frac{\phi_m}{1 - \phi_m} \right)^2 \left(\frac{1}{\xi^{1.5} \sigma_g^2} \right) \tag{27}$$

$$\frac{B}{\tau_y} = 0.066 \left(\frac{\phi_m^2}{\phi_m - \phi} \right) \left(\frac{\mu^2}{D_p^2 \rho_p \tau_y} \right)^{0.21} \tag{28}$$

$$\eta_\infty = \mu \exp \left\{ \left[2.5 + \left(\frac{\phi}{\phi_m - \phi} \right)^{0.48} \right] \frac{\phi}{\phi_m} \right\} \tag{29}$$

Values of τ_y, B, η_0/μ and η_∞/μ for the fourteen experimental systems were calculated from these equations and Equation (17). The calculated values of η_0/μ varied from about 35 to 3,500, and those for η_∞/μ varied from about 25 to 1,000. The computer program calculated values of the wall shear stress, τ_w, from Equation (23) and the calculated viscosity parameters for each of the 145 experimental runs. The curves in Figure 4 are for the calculated values of τ_w, and they illustrate the good agreement between the calculated and observed values. The standard error for the calculated value of τ_w was 10.8%. There appears to be a slight bias in the correlation curves toward lower values of wall shear stress at low shear rates. However, this is not the fault of the computer program in minimizing ψ in Equation (26). The bias results from the theoretical assumptions made in applying Equation (17) from the work of Landel (7), and in deriving Equations (1) and (27). These equations control the calculated value of τ_w at low shear rates. The curves fit the experimental data to within the accuracy of the determinations of ϕ and ϕ_m. The importance of obtaining high accuracy in these determinations may be observed from the large differences in τ_w for small differences in ϕ for the nickel-sodium, nickel-xylene, and aluminum-xylene systems in Figures 3 and 4.

Since the correlation was obtained from graphically determined values of G_w, Equation (23) was solved for G_w so that values of G_w could be calculated from given values of τ_w. Solving Equation (23) for G_w:

$$G_w = a_1 + a_2 \tau_w + a_2 \sqrt{\tau_w^2 + a_3 \tau_w + a_4} \tag{30}$$

where

$$a_1 = -1/2 \left[\frac{B g_c}{\eta_0 - \eta_\infty} + \frac{(\tau_y + B) g_c}{\eta_\infty} \right]$$

$$a_2 = \frac{g_c}{2\eta_\infty}$$

$$a_3 = 2 \left(\frac{B \eta_\infty}{\eta_0 - \eta_\infty} - \tau_y - B \right)$$

and

$$a_4 = \left(\tau_y + B + \frac{B \eta_\infty}{\eta_0 - \eta_\infty} \right)^2 - \frac{4 \eta_\infty B \tau_y}{\eta_0 - \eta_\infty}$$

The flow rate, Q, can be expressed in terms of G_w by solving Equations (21) and (22):

$$\frac{dR}{d\tau_w} + \frac{3R}{\tau_w} = \frac{4G_w}{\tau_w} \tag{31}$$

where $R = 32\, Q/\pi D^3$. Equation (31) can be solved for R with the boundary condition $R = 0$ at $\tau_w = \tau_y$:

$$R = \frac{4}{\tau_w^3} \int_{\tau_y}^{\tau_w} \tau_w^2 \, G_w \, d\tau_w \tag{32}$$

The integral in the above expression was evaluated by substitution of Equation (30), and straightforward analytical integration with the aid of a standard table of integrals. A mathematically simple, though very lengthy, expression resulted. Values of R and Q were calculated by computer from this expression for each of the 145 experimental runs. The input data were the observed values of τ_w, and the physical properties needed to calculate τ_y, B, η_0 and η_∞ from Equations (27), (28), (17), and (29), respectively. The results of this calculation are presented in the curves plotted in Figure 3. The shapes of the curves are very much like the curves of G_w vs. τ_w in Figure 4, except that the curves approach the τ_w axis asymptotically. This is required by the boundary conditions $R = 0$ and $G_w = 0$ at $\tau_w = \tau_y$, which results in $dR/d\tau_w = 0$ at $\tau_w = \tau_y$ when substituted in Equation (31).

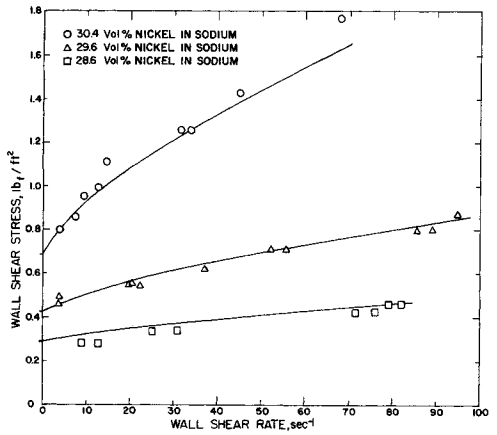

4a

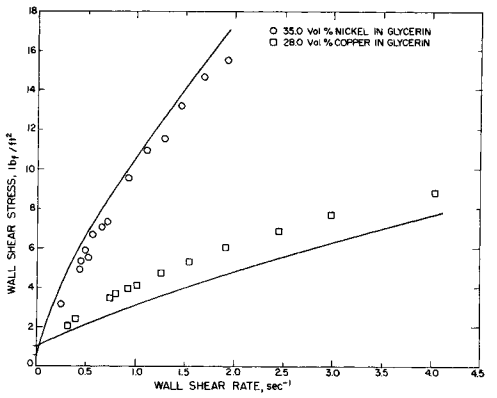

4b

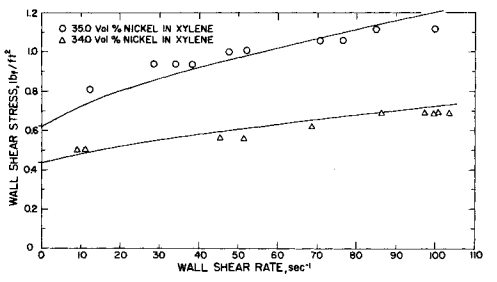

4c

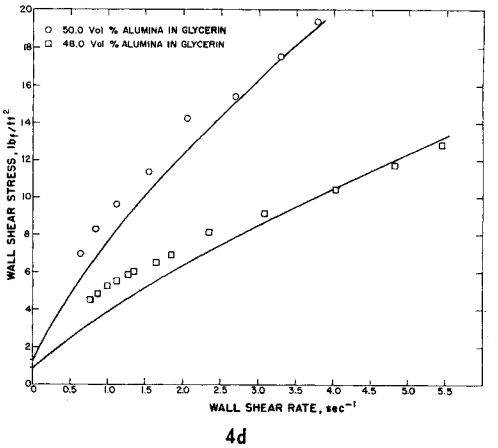

4d

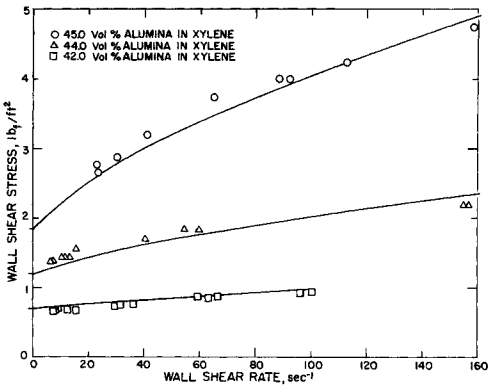

4e

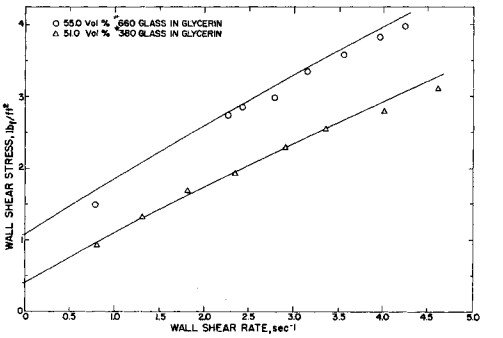

4f

Fig. 4. Wall shear stress vs. wall shear rate. The curves were calculated from Equation (23) and physical properties of the solids and vehicles.

APPLICATION OF RESULTS

The experimental data obtained in this investigation of high-solids suspensions cover wide ranges of physical properties of the liquid and the solid particles. Therefore, the correlation equations should be useful for many practical applications. For given values of pressure drop, liquid and solids properties, solid fraction, and maximum solid fraction, the flow rate may be calculated directly from Equation (32). This equation may be solved analytically, as was done in this investigation. Alternatively, Equation (32) can be solved by graphical integration, using arbitrary values of G_w and values of τ_w obtained from Equation (23).

The suspension flow measurements obtained in this research, and the development of the mathematical model were limited to the laminar flow region. The lowest value of η_∞ determined from the correlations was about 70 centipoise. High velocities would be required, even in large pipes, to reach turbulent flow for such viscous material. Alves, et al. (2), suggested that the pressure drop for turbulent flow of non-Newtonian materials may be determined from the friction factor as it is for Newtonian fluids. Also, it was recommended that the limiting viscosity for pseudoplastics at infinite shear (η_∞ in this investigation) be used in computing the Reynolds number.

The shear-stress vs. shear-rate equation, (Equation 23), was written for pipe flow, but it was shown (*11*) that this equation could be written in a tensorially invarient form involving the same viscosity parameters. Thus, the results of this investigation may be applied to geometrically complex flow systems.

CONCLUSIONS

The laminar flow behavior of high-solids suspensions is determined by the solids concentration and the physical properties of the particles and the vehicle.

In this investigation, it was found that high-solids suspensions exhibit a yield stress which is proportional to

the diameter of the particles and inversely proportional to the volume of free liquid, $\phi_m - \phi$. Other particle properties, namely the size distribution and shape, also have an effect on the yield stress. However, liquid properties, except as they affect the maximum solids fraction, have no apparent effect

There are three regions of flow on a shear-stress vs. shear-rate diagram for high-solids suspension: (a) a low shear-rate region in which the relative viscosity coefficient, η_0/μ, is a function of the ratio of solids volume fraction to the maximum solids fraction for the system, (b) an intermediate shear-rate region of pseudoplastic flow in which the viscosity coefficient is a complex function of both liquid and solids properties, and (c) a high shear-rate region in which the relative viscosity coefficient η_∞/μ, is again a function only of the ratio of the solids fraction to the maximum solids fraction.

The above flow behavior can be predicted quantitatively for a wide range of suspensions by the correlation equations derived in this study. These correlation equations require data on easily measured properties of the solids, the vehicle, and the solids fraction and maximum solids fraction of the suspension.

ACKNOWLEDGMENT

The authors are grateful for the suggestions of Professor Edward Bagley of Washington University during the course of the experiments, and in ahe writing of the paper. Dr. Melvin S. Foster devised the computer program for correlating the data.

NOTATION

a = shape factor in Vand equation
A = factor in yield stress equation, lb.$_f$/cu.ft.
b = Rabinowitsch constant
B = flow parameter, lb.$_f$/sq.ft.
C = constant of proportionality
D = test-pipe flow diameter, in.
D_p = particle diameter. [In Equations (27) and (28), D_p = geometric mean diameter], ft.
f = two-body collision frequency per unit volume, sec.$^{-1}$ ft.$^{-3}$
F_s = force necessary to overcome interparticle contact, lb.$_f$
G = $-dv/dr$ = shear rate, sec.$^{-1}$
G_w = shear rate at the wall, sec.$^{-1}$
g_c = force-mass conversion factor, (lb.$_m$/lb.$_f$) (ft./sec.^{2})
k = dimensionless constant
K = rate constant, cu.ft./sec.
l = dimensionless constant
L = pipe length, ft.
m = dimensionless constant
n = dimensionless constant
N = number of particles per unit volume
n_c = number of particle-particle contacts per unit volume
ΔP = test-pipe pressure differential, lb.$_f$/sq.in.
Q = volume flow rate, cu.in./sec.
R = flow parameter $32Q/\pi D^3$, sec.$^{-1}$
r = radial pipe direction, ft.
t_c = time spent by one sphere in collision with other spheres, sec.
z = axial pipe direction, ft.
dv/dr = velocity gradient in the axial direction of the pipe, sec.$^{-1}$

Greek Letters

β = rate constant, sec.$^{-1}$
β_0 = rate constant, sec.$^{-1}$
β_1 = rate constant, dimensionless
η = suspension viscosity, lb.$_m$/sec.-ft.
η_r = relative viscosity (ratio of suspension viscosity to liquid viscosity)
η_0 = viscosity parameter at low shear rates, lb.$_m$/sec.-ft.
η_∞ = viscosity parameter at high shear rates, lb.$_m$/sec.-ft.
θ = shear stress necessary to overcome particle-particle contacts, lb.$_f$/sq.ft.
μ = liquid vehicle viscosity, lb.$_m$/sec.-ft.
ξ = shape factor defined as the ratio of the surface area of a sphere of equivalent volume to the surface area of the particle
ρ_p = suspension density, lb.$_m$/cu.ft.
σ_g = geometric standard deviation for particle diameter
τ_i = intercept on the shear-stress axis of shear-stress vs. shear rate relationship for high shear rates [Equation (24)], lb.$_f$/cu.ft.
τ_{rz} = shear stress in the axial direction, z, of the test pipe, and at a distance, r, from the axis, lb.$_f$/sq.ft.
τ_w = suspension yield stress at the pipe wall, lb.$_f$/sq.ft.
τ_y = suspension yield stress, lb.$_f$/sq.ft.
ϕ = volume fraction solids
ϕ_m = maximum obtainable volume fraction solids for the system
ψ = correlation function defined by Equation (26)

LITERATURE CITED

1. Metzner, A. B., and J. C. Reed, *AIChE J.*, **1**, 434 (1955).
2. Alves, G. E., D. F. Boucher, and R. L. Pigford, *Chem. Eng. Progr.*, **48**, 385 (1952).
3. Skelland, A. H. P., "Non-Newtonian Flow and Heat Transfer," John Wiley, New York (1967).
4. Robinson, J. V., *J. Phys. Colloid Chem.*, **53**, 1042 (1949).
5. Vand, V., *ibid.*, **52**, 277 (1948).
6. Mooney, M., *J. Colloid Sci.*, **6**, 162 (1951).
7. Landel, R. F., B. G. Moser, and A. J. Bauman, *Proc. Intern. Congr. Rheol. 4th*, 663, New York (1965).
8. Williams, P. S., *J. Appl. Chem.*, **3**, 120 (March, 1953).
9. Thomas, D. G., *AIChE J.*, **7**, 431 (1961).
10. Ibid, **9**, 310 (1963).
11. Gay, E. C., Ph.D. thesis, Washington Univ., St. Louis, Mo. (1967).
12. Crowley, P. R., and A. S. Kitzes, *Ind. Eng. Chem.*, **49**, 888 (1957).
13. Hanks, R. W., *AIChE J.*, **9**, 306 (1963).
14. Murdoch, R., and H. A. Kearsey, *Trans. Inst. Chem. Eng. (London)*, **38**, 165 (1960).
15. Goodeve, C. F., *Trans. Faraday Soc.*, **35** (1939).
16. Manley, R. St. J., and S. G. Mason, *J. Colloid Sci.*, **7**, 354 (1952).
17. Bogue, D. C., *Ind. Eng. Chem.*, **51**, 874 (1959).
18. Mooney, Melvin, *J. Rheol.*, **2**, 210 (1931).
19. Reiner, Markus, 'Deformation, Strain, and Flow," 2nd Ed., Interscience, New York (1960).
20. Vand, Vladimir, *J. Phys. Colloid Chem.*, **52**, 300 (1948).
21. Maude, A. D., and R. L. Whitmore, *Brit. J. Appl. Phys.*, 7, 98 (1956).
22. Thomas, D. G., *AIChE J.*, **6**, 631 (1960).
23. Burgers, J. M., and G. W. Scott Blair, *Proc. Intern. Congr. Rheol.*, North Holland Publishers, Amsterdam (1948).
24. Ulrich, W. F., *Analyzer*, **2**, (1961).
25. Nelsen, F. M., and F. T. Eggertsen, *Anal. Chem.*, **30**, 1387 (1958).
26. Berg, R. H., *Amer. Soc. Testing Mater. Spec. Tech. Publ.*, **234**, 245 (1958).
27. Smith, J. E., and M. L. Jordan, *J. Colloid Sci.*, **19**, 549 (1964).
28. Metzner, A. B., and J. C. Reed, *AIChE J.*, **1**, 434 (1955).
29. Marquardt, D. W., *J. Soc. Ind. Appl. Math.*, **2**, 431 (1963).

Manuscript received March 22, 1968; revision received June 21, 1968; paper accepted June 26, 1968.